

Article

Wear and Optical Properties of MoSi₂ Nanoparticles Incorporated into Black PEO Coating on TC4 Alloy

Hao Zhang ^{1,2,*}, Jiayi Zhu ², Jingpeng Xia ², Shang Sun ² and Jiaping Han ^{2,*}¹ National Engineering Research Center for Biomaterials, Sichuan University, Chengdu 610064, China² Institute of Vanadium and Titanium, Panzhihua University, Panzhihua 617000, China

* Correspondence: zhanghaozi25@163.com (H.Z.); hanjiaping88@126.com (J.H.)

Abstract: Wear resistance and optical properties are the key point for the application of titanium alloys as structural materials in the aerospace field. To enhance the wear resistance and optical properties of titanium alloys, a black plasma electrolytic oxidation (PEO) coating incorporating MoSi₂ nanoparticles was fabricated on the TC4 alloy via the PEO process, with the MoSi₂ nanoparticles being in situ doped into the coating. The doping of MoSi₂ nano-particles can effectively reduce the pore size of the PEO layer. The nPEO coating exhibited lower surface roughness than that of the PEO layer. The surface hardness of the nPEO coating increased to 42.5 HRC, significantly enhancing the wear resistance of the PEO layer (40.7 HRC). Furthermore, the PEO coatings exhibited better optical property compared to TC alloy, and the incorporation of MoSi₂ particles further improved the performance in most wavelength ranges. The infrared emissivity of the nPEO coating was 0.87, a dramatic increase from the 0.38 value of the TC4 alloy. This coating strategy effectively enhances the wear resistance and optical performance of TC4 alloy, which is critical for the surface design of titanium alloys used in aerospace applications.

Keywords: black coating; PEO; nanoparticles; wear resistance; optical property; Ti alloy



Academic Editor: Hideyuki Murakami

Received: 5 December 2024

Revised: 19 December 2024

Accepted: 27 December 2024

Published: 29 December 2024

Citation: Zhang, H.; Zhu, J.; Xia, J.; Sun, S.; Han, J. Wear and Optical Properties of MoSi₂ Nanoparticles Incorporated into Black PEO Coating on TC4 Alloy. *Coatings* **2025**, *15*, 21. <https://doi.org/10.3390/coatings15010021>

Copyright: © 2024 by the authors. Licensee MDPI, Basel, Switzerland. This article is an open access article distributed under the terms and conditions of the Creative Commons Attribution (CC BY) license (<https://creativecommons.org/licenses/by/4.0/>).

1. Introduction

Titanium alloy has the advantages of low density, high specific strength and high corrosion resistance, thus is widely used in the aerospace field [1,2]. At present, the proportion of titanium alloy in aircraft, especially in fighter jets, is becoming larger. However, the performance of titanium alloy at high temperatures (exceeding 600 °C) is relatively poor [3]. In addition to the rapid oxidation rate, low hardness and poor wear resistance is also the main reason for its failure [4]. In addition, the optical properties of aircraft structural materials are closely related to their concealment properties, which is also an important factor to be considered. Light absorption and emissivity of titanium alloy are reported to be quite low [5]. How to improve the wear resistance and optical properties is crucial to promote the application of titanium alloy.

Performing a tinted coating is a recently developed approach to fulfill the requirement of the optical properties. Various tinted coatings were fabricated on the surface of metal-based materials, while various agents were employed to confer different colors [6,7]. The tinted coatings improve aesthetics and have a function of decoration [8]. The enhanced optical properties are beneficial to improve the concealment effect of the matrix [9]. Plasma electrolytic oxidized (PEO) coatings exhibit superior performance in various preparation methods of colored coatings [10]. Ceramic coatings have excellent corrosion and wear resistance, and good adhesion with matrix due to the in situ formation process. However,

intrinsic porous morphology increases surface roughness, together with the existence of defects and discharge channels in the coatings, leading to a deterioration of wear resistance.

Considering the high performance requirements of tinting PEO coating, further improving the performance is imperative. In addition to adjusting the electrical parameters and electrolyte composition, in situ doping of nano-reinforced particles in the PEO layer has been a common strengthening method. The PEO coating can be multi-functionalized by doping particles with different physiochemical properties, thus improving its biological, corrosion resistance, wear resistance and other properties, etc. [11,12]. M. Nadimi et al. [13] prepared ZnO-ZrO₂ nanoparticles incorporated with PEO coating on TC4 alloy, and the addition of particles modified the morphology and had a positive effect in improving the corrosion and antibacterial property of PEO coating. Sidra et al. [14] selected MoS₂ nanoparticles as a reinforcement of PEO coating on TC4 alloy. PEO coating with the inclusion of MoS₂ nanoparticles displayed superior corrosion resistance and cell proliferation property. Other reinforcements, including hydroxyapatite (HA), SiO₂, Ta₂O₅, TiO₂, and lanthanum manganite, have already reported to be in situ incorporated into PEO coatings on Ti alloys, and the properties of PEO coatings were remarkably enhanced [15–18]. MoSi₂ nanoparticles possess relatively high hardness and excellent high-temperature stability [19,20]. A smooth surface can be obtained via MoSi₂ inclusion which benefited in improving the wear resistance [21]. Therefore, it is an ideal candidate as a reinforced particle for PEO treatment.

However, MoSi₂ nanoparticles have not been reported in situ incorporated into a PEO coating. The incorporation of the MoSi₂ nanoparticles on the coating formation and properties is indispensable to be revealed, and the synergistic effect of the particles and coloring agent is also required to be investigated. In the present work, black PEO coating was introduced on Ti alloy to enhance the wear and optical properties, and MoSi₂ nanoparticles were incorporated into the coatings to further improve the performance. The black PEO coating was systematically characterized, the wear and optical properties were investigated, and the influence of the incorporation of MoSi₂ nanoparticles on the morphology and properties of PEO coating was discussed in detail.

2. Experimental

2.1. PEO Process

Commercial TC4 alloy ($\geq 99.9\%$) was employed in the present study. The specimens were wire-electrode-cut into a size of $15 \times 15 \times 4 \text{ mm}^3$, then polished by SiC abrasive paper from 400 to 1200 grids. A black PEO coating was fabricated and 5 g/L FeSO₄ and Ni(CH₃COO)₂·4H₂O were utilized as color agents. A titanium plate was used as the cathode, and the polished TC4 specimens were the anode. The basic electrolyte contained 15 g/L (NaPO₃)₆, 30 g/L EDTA-2Na, and 0.5 g/L MoSi₂ nanoparticles were added into the electrolyte. To ensure the uniform distribution of the nanoparticles, the electrolyte was firstly ultrasonic treated for 30 min, and then stirred at the rate of 300 r/min during the whole deposition period. The PEO process was carried out under a current constant mode at 0.2 A/cm². The terminal applied voltage was settled as 400 V and the whole oxidation period lasted for 20 min with a frequency of 500 Hz and duty circle of 10%, respectively. The obtained sample was labeled as nPEO. To investigate the impact of MoSi₂ nanoparticles on the coating properties, a PEO layer was fabricated using an electrolyte without MoSi₂ nanoparticles simultaneously for comparison.

2.2. Coating Characterization

The morphology and elemental composition of the coatings were analyzed by scanning electron microscope (SEM, Tescan, Hamburg, Germany) equipped with EDS detector, under 15 kV accelerated voltage. Surface topography and roughness (R_a) of coatings were

investigated by atomic force microscope AFM and laser confocal microscopy (FV1200, Olympus Corporation, Tokyo, Japan). The phase composition of Ti and PEO coatings was analyzed by Bruker D8 Advance diffractometer using a Cu K α radiation source at 40 kV and 40 mA. The scanning range was from 10° to 80° with a scanning rate of 0.01°/s. Vickers hardness was measured at room temperature, six points were selected for each specimen, and the average of six values was adopted to determine the final hardness values. Surface porosity of PEO coatings was calculated by Image J image processing software (fiji w7).

2.3. Dry Sliding Wear Tests

The dry sliding wear tests of Ti alloy and PEO coatings were performed with a Tribotec oscillating tribometer. A stainless steel ball of 6 mm diameter served as friction partner. The wear tests were carried out at a sliding speed of 5 mm/s under 5 N load with oscillating amplitude of 10 mm. The tests lasted for 40 min while ambient conditions were controlled at 25 ± 2 °C and 30% r.h. by a temperature-regulating device; 3D morphology and profile of the wear tracks was monitored via laser scanning confocal microscope (LSCM) after the wear tests.

2.4. Optical Measurements

The optical properties of the specimens were measured employing an infrared emissivity tester (TSS-5X) and infrared diffuse reflection tester (Shimadzu UV-3600i Plus, Kyoto, Japan) at room temperature. The wavelength of infrared emissivity was 4–22 μm , and the length of absorptivity was 200–2500 μm . For the tests, the accuracy was controlled at ± 0.01 at the detection distance of 12 mm. The data were acquired every 2 nm at a mediate scanning rate. Each test was carried out three times to ensure the repeatability.

3. Results and Discussion

3.1. Coating Characterization

Phase composition of the PEO coatings was examined and the diffraction peaks of TC4 alloy were also listed as a contrast, as shown in Figure 1. Identified in a standard PDF card (44–1294), all of the diffraction peaks belonged to TC4 matrix, and no additional peaks of PEO coatings were detected. An unclear, wide bulk appeared at the range of 25° to 35°. The corresponding diffraction intensity of Ti matrix decreased to a certain extent for the PEO coatings, suggesting the existence of the PEO coatings. Fe and Ni elements are magnetic materials that have a negative influence on XRD detection and always generate indistinct diffraction peaks [22]. This might be also concerned with the formed amorphous structure of the PEO coating, as proved by the existence of wide bulks in the patterns of PEO and nPEO coatings. The incorporation of the Si element may intensify the formation of the amorphous phase, as reported by Han et al. [23].

Surface morphology was affected after the incorporation of MoSi₂ nanoparticles, as shown in Figure 2; local elemental analysis of the respective coatings are listed in Table 1. Typical volcano morphology appeared as a result of intensive discharge and the effusion of a large amount of gas. Some cracks and defects existed in both coatings which were produced by the quenching effect of the electrolyte. Micro pores uniformly distributed on PEO surface, and there was limited difference in the dimension of micro pores. More micro pores could be observed on the surface of the nPEO coating, and the average size of the pores seemed to decrease slightly after the incorporation of the nanoparticles. O, Ti, P, and a small amount of Fe element were detected in the PEO and nPEO coatings, which originated from the Ti matrix and the electrolyte. Aggregated regions of Si and Mo elements appeared in the nPEO coating due to the incorporation of MoSi₂ particles.

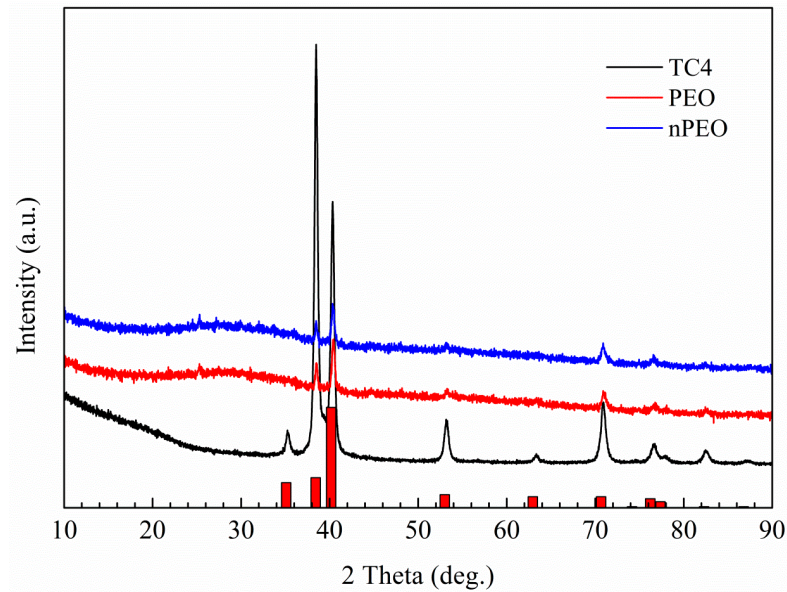


Figure 1. XRD patterns of TC4 alloy and the PEO coatings after 20 min of deposition.

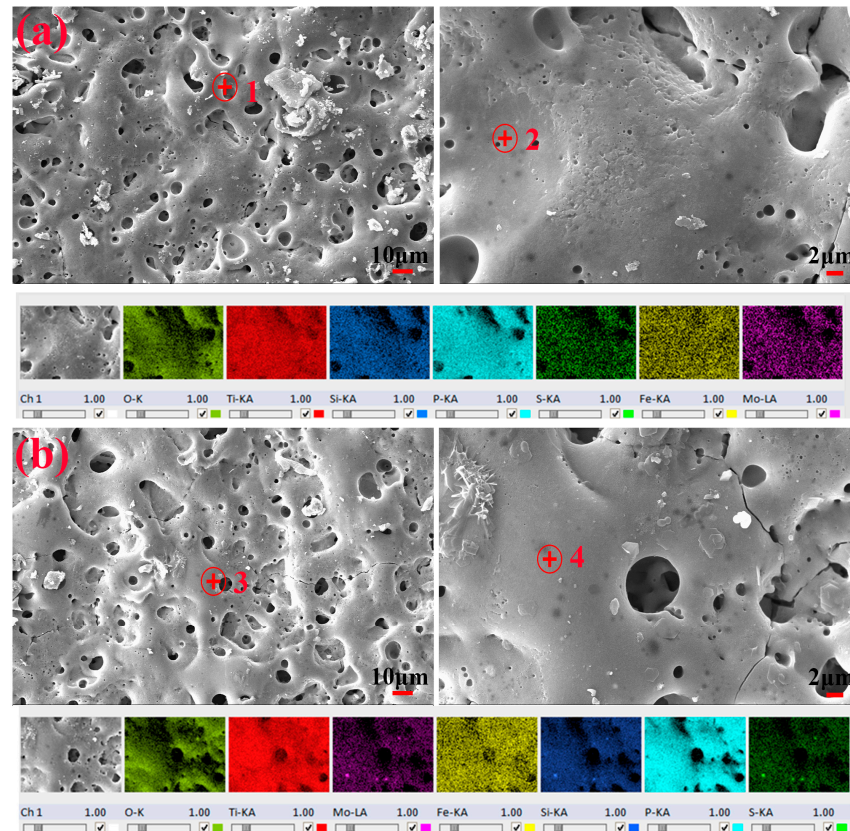


Figure 2. Surface morphology and elemental mappings of the PEO coatings after 20 min of deposition. (a) PEO and (b) nPEO, the numbers was the selected region for elemental analysis.

The observed elements help to understand the composition of the coating system and also certified the incorporation of the nanoparticles. The difference in composition, as well as in the morphology, resulted in different performance characteristics. In the present work, O, P, Ti, and Fe elements were found in both PEO coatings. O and P originated from the electrolyte and Ti was from the Ti matrix, which composed the basic composition of the PEO layer. Fe normally gives ferromagnetic properties to the Ti-sample, and also colors the PEO coating in the present work. The addition of Fe always resulted in crystallites,

which may be responsible for the undetectable peaks in XRD measurement [24]. Si and Mo existed in nPEO coating, suggesting the successful incorporation of MoSi₂ particles. The incorporation of MoSi₂ particles reduced the surface roughness and improved the surface hardness, thus enhancing the wear performance of the PEO coating. Normally the decrease in surface roughness may lead to a decrease in optical property. However, the incorporation of MoSi₂ particles slightly improved the optical property while decreasing the surface roughness. It can be inferred that MoSi₂ particles had a positive effect in improving the optical property.

Table 1. Local elemental analysis (wt.%) of surface and cross-section morphology of PEO coatings.

Sample	Position	Region	O	Si	P	Ti	Fe	Mo
PEO	Surface	1	63.1	0.14	18.56	16.92	1.16	0
		2	65.77	0.18	17.2	15.12	1.26	0
	Cross-section	1	65.3	0.05	18.21	15.23	0.85	0
		2	71.3	0.08	8.32	20.25	0.34	0
nPEO	Surface	3	56.5	2.84	18.61	19.8	1.91	0.34
		4	53.04	3.71	20.82	20.34	1.9	0.17
	Cross-section	3	57.68	3.03	20.32	16.78	1.85	0.28
		4	68.21	1.36	7.85	19.98	0.96	0.13

To further understand the effect of in situ incorporated nanoparticles on the morphology of the PEO coating, AFM and LSCM were employed to characterize the surface morphology and evaluate the surface roughness, as shown in Figure 3. R_a values were obtained by both AFM and LSCM measurements. A wider range of local regions was scanned by LSCM (2560 $\mu\text{m} \times 2560 \mu\text{m}$) than that of AFM (100 $\mu\text{m} \times 100 \mu\text{m}$). A wider range of local regions was scanned by LSCM than that of AFM. Abrasion scratches can be clearly observed on the surface of Ti alloy (Figure 3a). A relatively smooth surface was presented, with R_a values of 455 nm and 3.685 μm , respectively. Rough surfaces were introduced after PEO processing. Micro pores can be clearly featured in both PEO coatings. The R_a values of the PEO coating increased to 1.063 μm and 8.307 μm , respectively. After the incorporation of nanoparticles, the values decreased slightly, indicating that the incorporation of MoSi₂ resulted in a lower surface roughness.

The porosity and average pore size were quantitatively calculated by image J software in determined regions and the results are shown in Figure 4. The porosity increased slightly after loading the particles, from 7.9% to 8.2%. However, the average pore size decreased noticeably from 4.9 μm to 3.6 μm . The incorporation of nanoparticles had a positive effect in reducing the pore size. This phenomenon was always reported in particle-incorporated PEO coatings. A common interpretation is concerned with the Zeta potential of the particles in the electrolyte and the physiochemical properties of the employed particles. Normally, particles present electronegativity in the electrolyte and move toward the anode (specimens) under the electric field force. Normally, particles present electronegativity in the electrolyte and move toward the anode (specimens) under the electric field force, as certified by Han et al. [25]. The attachment of the particles at the interface somehow inhibits the uniform discharge of the PEO process. Higher breakdown potential is required in the particle-adhered region, which leads to non-uniform discharge in local regions. Higher Zeta potential means better distribution of the particles in the electrolyte, as well as more uniformly adhered on the surface during the PEO process [26]. This has a more positive effect on reducing the pore size. Meanwhile, the addition of

non-conductive particles normally leads to a decrease in the conductivity of the electrolyte and impedes the voltage response to some extent, which also might result in a decreased pore size. In most cases, the decrease in pore size would result in an improvement in wear resistance, and the smaller the pore size was, the better wear performance was presented, as also revealed by Babak et al. [27]. Two reasons are responsible for the improvement: The first is the decrease in surface roughness, another is the increasing compactness of the PEO layer accompanied by the decreasing pore size and porosity. As to the optical property, the film with an average pore size of $0.45\ \mu\text{m}$ offers excellent spectral selectivity, as reported by Zhu et al. [28]. The average size of micro pores in the present work was larger than this value. The average size of the PEO coating was $4.9\ \mu\text{m}$ and $3.6\ \mu\text{m}$ for the nPEO coating. A smaller value of nPEO coating may also contribute to a higher optical property.

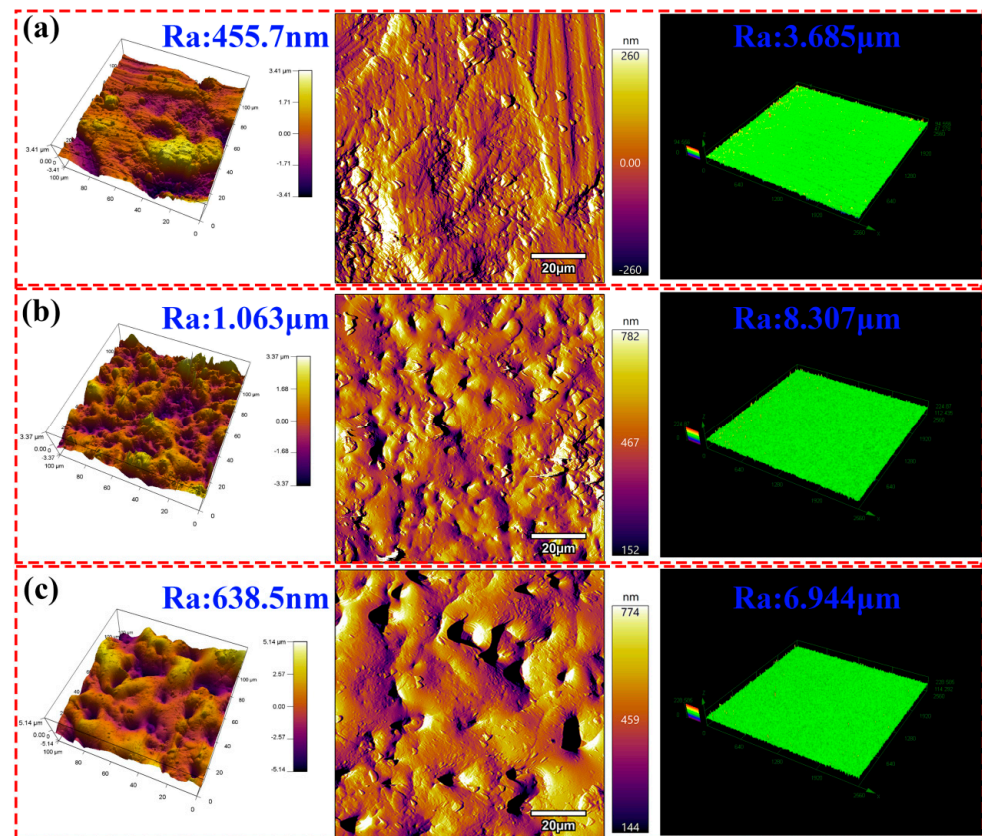


Figure 3. Surface characteristics of TC4 alloy and the PEO coatings given by AFM and LSCM. (a) TC4, (b) PEO coating, (c) nPEO coating.

Cross-section morphology intuitively reflected to change in coating thickness and morphology after the incorporation of MoSi_2 particles, as shown in Figure 5. The local elemental analysis was also listed in Table 1. Besides the defects, open pores, and discharge channels, two layers can be clearly distinguished in both cross-section morphologies: the outer porous layer and the inner compact layer. The thickness of PEO and nPEO coatings was approx. $15\ \mu\text{m}$ and $13\ \mu\text{m}$, respectively. The thickness of the coating decreased due to a delay in voltage response. Micro pores were uniformly distributed in PEO coatings, while a big difference existed in the pore size of the nPEO coating. Several large pores ($\geq 5\ \mu\text{m}$) and a considerable amount of smaller pores ($\leq 1\ \mu\text{m}$) can be observed. More micro pores with smaller sizes were generated, and the pores presented non-uniform distribution. Meanwhile, the composition of the outer porous layer and inner compact layer showed obvious differences, as summarized in Table 1. Ti and O elements were the main composition of the inner layer, while the content of the P and Fe elements increased

noticeably in the outer layer. This was more concerned with the formation mechanism of PEO coatings. The inner compact layer formed in the general oxidation stage, and the oxide of the matrix materials was preferentially formed in this period. Afterwards, the outer layer was deposited in a later stage, and more components in the electrolyte participated in the coating formation process, and the content of P and Fe elements increased accordingly. The content of MoSi_2 particles also increased with the prolongation of the deposition time, and more particles moved toward the anode under higher transient voltage.

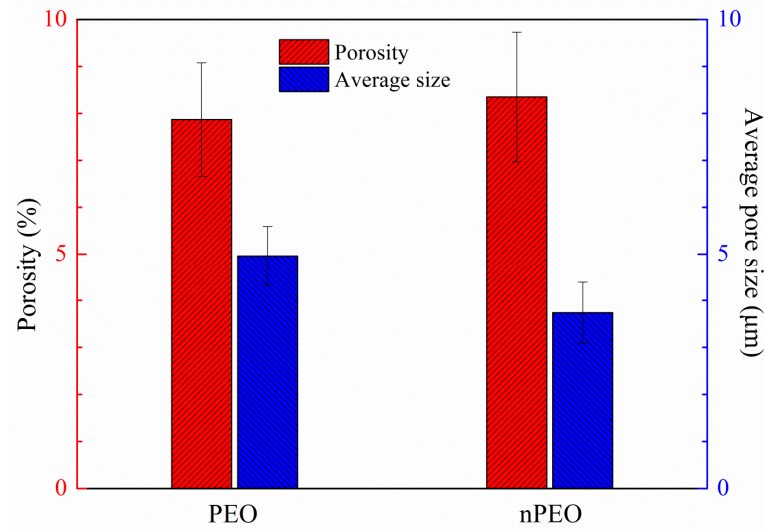


Figure 4. Porosity and average pore size of the PEO coatings after 20 min of deposition.

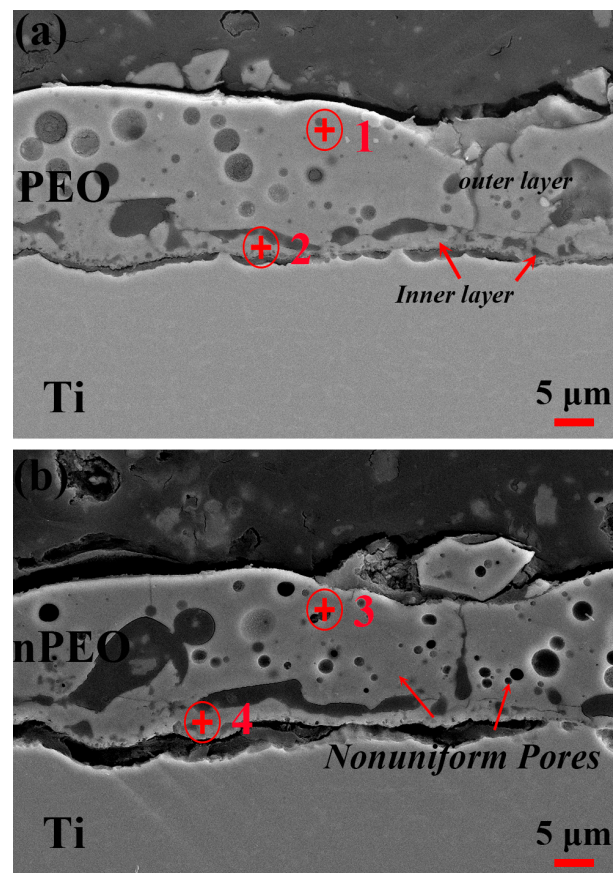


Figure 5. Cross-section morphology of the PEO coatings after 20 min of deposition. (a) PEO coating and (b) nPEO coating, the numbers was the selected region for elemental analysis.

3.2. Wear Performance

The friction coefficient of the titanium matrix and PEO coatings is shown in Figure 6. The initial friction coefficient of titanium alloy was relatively low, about 0.32. This might be a result of considerable hardness and the smooth surface after polishing. With the increase in friction time, the friction coefficient of titanium alloy gradually increased to 0.42, which may be caused by the continuous accumulation of wear products on the surface hindering the sliding of the steel ball. After PEO treatment, the initial friction coefficient of the surface increased to 0.44 and 0.41, respectively, which may be caused by the increase in surface roughness introduced by the PEO layer. The friction coefficient of the coating was basically constant during the whole test cycle, indicating that the coating played an effective role in protecting the matrix. The friction coefficient of the nPEO coating with nanoparticles added was lower than that of the bare PEO coating, which may be related to the increased hardness and reduced surface roughness.

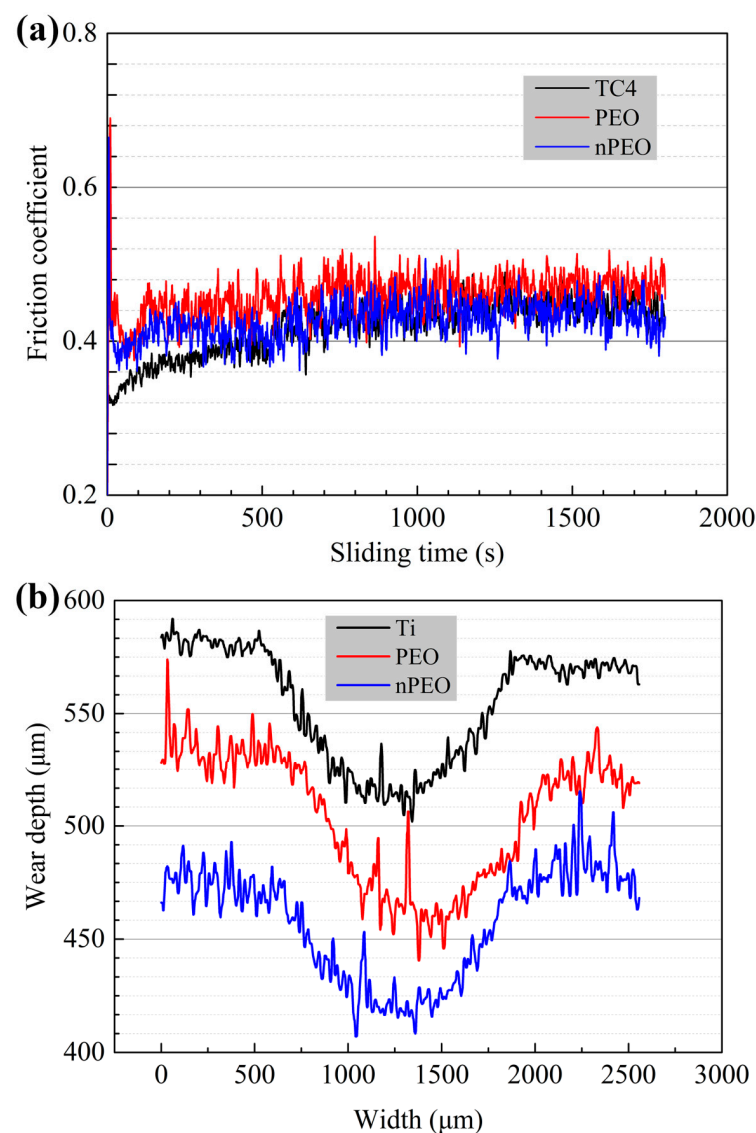


Figure 6. Friction coefficient of the specimens and the characteristics of the wear tracks. (a) Friction coefficient and (b) the characteristics of the wear tracks.

The scratch width and depth of the three specimens are shown in Figure 6b, and the accurate values are displayed in Figure 7a. The width of the three scratches was slightly different. The value of titanium alloy (1350 μm) and nPEO (1090 μm) was significantly

smaller than that of PEO coating (1425 μm). There also existed a difference in the depth of the scratches. The scratch depth of titanium alloy was about 75–80 μm , and the scratch depth of PEO and nPEO coating was 81 μm and 67 μm , respectively. The wear resistance of the PEO layer was noticeably improved by the addition of nanoparticles. The surface hardness value was also an important factor that determined the wear performance, as shown in Figure 7b. The hardness value of TC4 alloy was 36.2 HRC. Ceramic PEO coatings presented higher hardness, with a value of 40.7 HRC. The hardness further improved after the incorporation of MoSi_2 particles, and the value increased to 42.5 HRC.

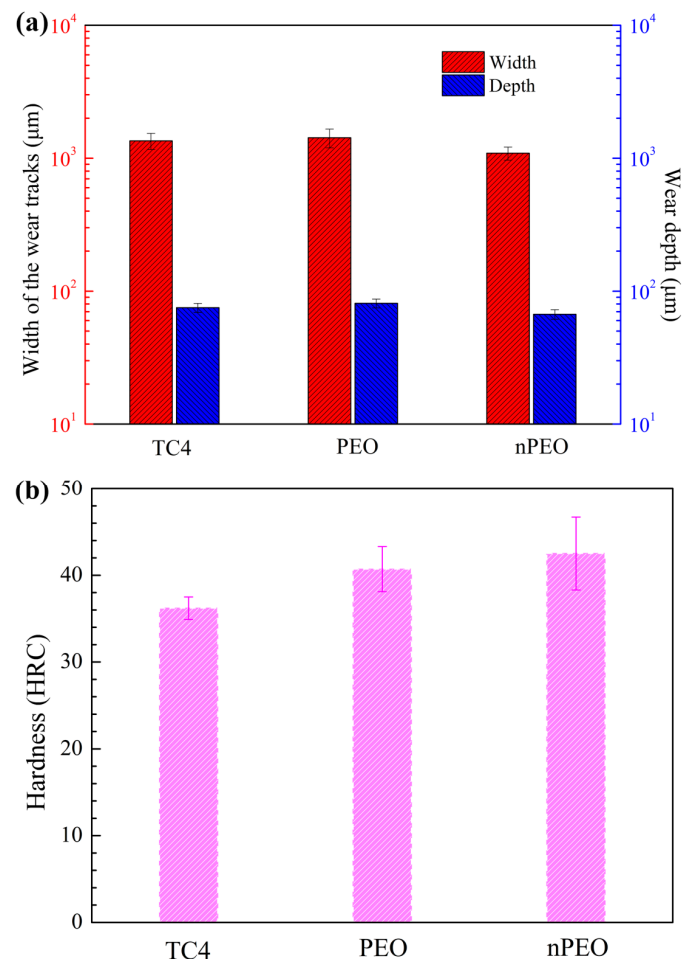


Figure 7. Wear depth and width of the wear tracks and the surface hardness. (a) Wear depth and width and (b) surface hardness.

The three-dimensional topography showed that the scale of PEO coating was larger than that of Ti alloy (Figure 8), but this did not reflect the true scratch depth, due to the large surface roughness value of PEO coatings. The approximate color of the scratch and the surrounding scratch was helpful in determining the values, and the data in the outline were more accurate. It can be seen from Figure 8 that the width of the scratch on the surface of the titanium alloy was not evenly distributed, and the highest plane position was distributed on both sides of the scratch, mainly concerned that the titanium alloy matrix caused plastic deformation during the friction process, and the titanium matrix was squeezed to both sides. The width and depth of scratches on the surface of PEO and nPEO coatings were relatively uniform, and there was no obvious plastic deformation trace on both sides of the scratches. Strips of bumps among the scratches survived on the surface which seemed to be the leftover coating or substrate. The scratch was more like being flaked than squeezed.

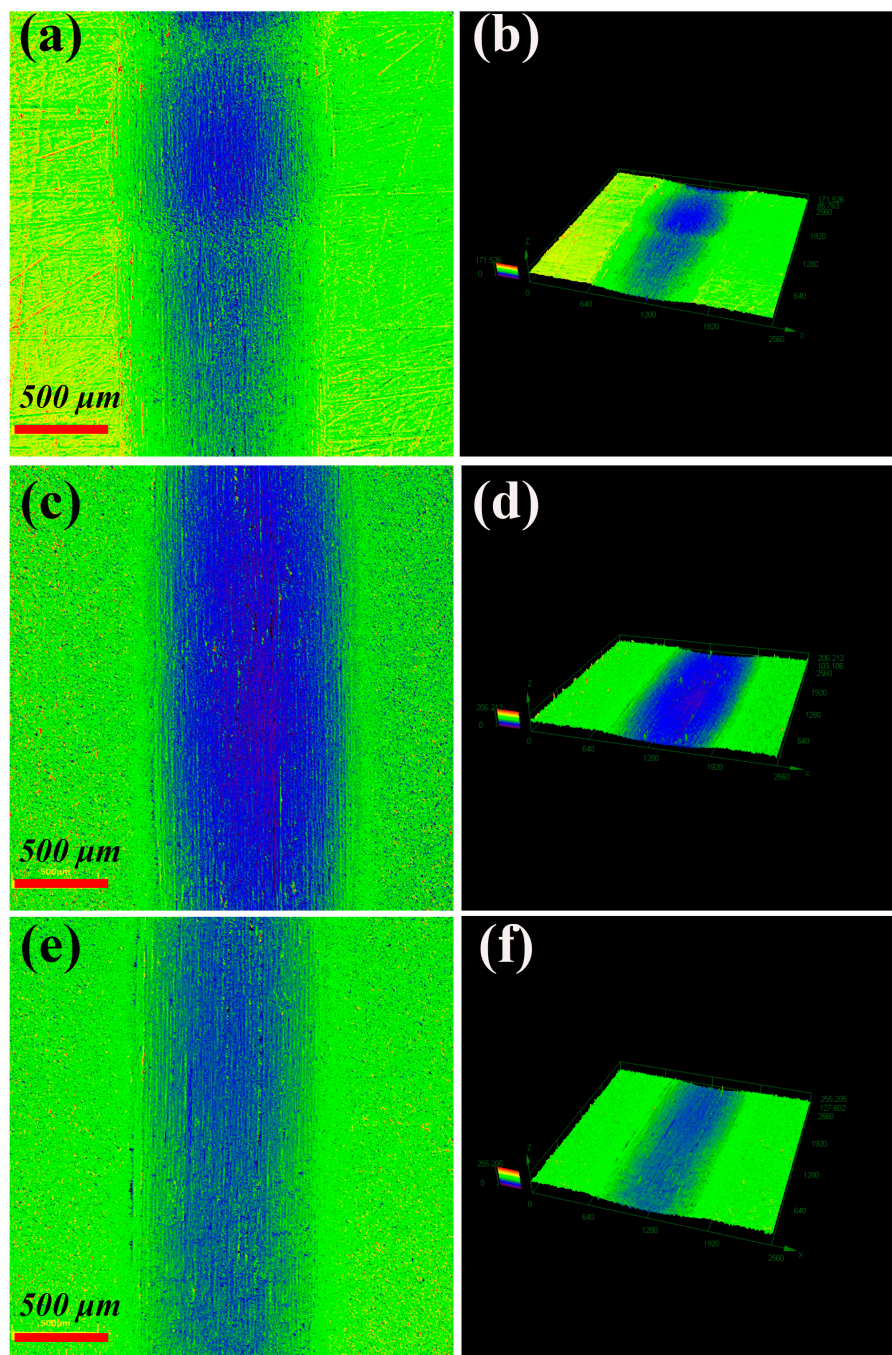


Figure 8. Three-dimensional wear tracks of TC4 alloy and the PEO coatings. (a,b) TC4 alloy, (c,d) PEO coating, and (e,f) nPEO coating.

Two factors play an important role in the wear performance of the materials (including coatings): hardness and surface roughness [29]. TC4 alloy possesses a relatively smooth surface after polishing, as proved by the lowest R_a value. The lowest friction coefficient is presented accordingly though the hardness of the Ti alloy is lower than the PEO coatings. Interestingly, wear tracks of Ti alloy were inconsistent along the length direction, as seen in Figure 8. This is mainly caused by the plastic deformation of the Ti matrix. The Ti matrix is squeezed along the direction of the sliding partner travels, and generates an uneven surface in the wear tracks. The different sliding conditions in local regions introduce additional sliding resistance against the partner. Thus, a non-uniform wear track is presented on the TC4 surface (Figure 8a). The deformation of the Ti matrix, as well as the accumulation

of friction debris, results in a relatively uneven surface, which leads to an increasing friction coefficient.

Ceramic PEO coating exhibits a higher hardness value but lower plastic deformation ability. The coatings suffer exfoliation more than deformation during the sliding process. This ensures the surface stability to some extent, and a relatively uniform wear track can be observed in Figure 8c,e. The largest surface roughness of PEO coatings leads to the highest friction coefficient, as well as the largest wear depth and width values.

Normally, the wear property is more concerned with the surface roughness and hardness [30]. The enhancement of particle incorporation in wear resistance is manifested in the following aspects. The first aspect is to increase the hardness value. MoSi₂ particles possess relatively high hardness which benefits in improving the coating hardness. In addition, the incorporation of particles reduces the average pore size of the outer PEO layer, which increases the compactness of the PEO layer to some extent, which also increases the hardness value of the coating. The decrease in surface roughness is another factor that enhances the wear resistance. Intensive discharge is inhibited due to the incorporation of particles, as discussed above, which introduces a smoother surface compared to the coatings which are particle-free. A relatively shallow wear track is performed in Figure 8e,f, proving excellent wear resistance of the MoSi₂-incorporated coating.

3.3. Optical Property

Black PEO coating was fabricated on the TC4 surface with the aim of improving its optical property. Absorptivity and infrared emissivity of the TC4 alloy and the two PEO coatings are shown in Figure 9. The PEO coatings remarkably improved the performance of the Ti matrix. The absorptivity of the PEO coatings was noticeably higher than that of the TC4 matrix at the wavelength ranging from 200 μm to 2000 μm, and presented lower values from 2000 μm to 2500 μm, as shown in Figure 9a. The infrared emissivity of TC4 alloy was merely 0.38, then dramatically increased to 0.84 after PEO treatment. The values further improved to 0.87 after the incorporation of MoSi₂ particles.

The wear performance of the coatings was basically determined by surface roughness R_a and the surface hardness. In the present work, R_a was determined by AFM and LSCM, respectively. R_a of Ti alloy was 455.5 nm and 3.685 μm, which led to a relatively low friction coefficient. The deformation in local regions during the friction process changed the real R_a in wear tracks, thus the friction coefficient increased gradually. R_a of the PEO coating (1.063 μm and 8.307 μm) was higher than that of the nPEO coating (638.5 nm and 6.944 μm), and poorer wear resistance was presented. Meanwhile, the disparity in surface roughness has a different effect on the absorption and emission behaviors of the coatings. The lowest R_a values of Ti alloy resulted in the poorest optical property, and a noticeable improvement can be identified in Figure 9 after PEO processing.

Many factors co-effect on the optical properties of the system. Besides the external conditions, such as temperature, pressure, and wavelength, physiochemical properties of the materials determines the optical performance. Ceramic materials normally present higher absorptivity and infrared emissivity than metal materials, thus PEO coatings exhibit better optical performance than TC4 alloy [31]. It can be inferred that MoSi₂ particles benefit in improving the optical properties. In addition, the optical property is concerned with the surface state [32]. A rough surface facilitates in production of higher absorptivity and infrared emissivity. The PEO coatings exhibit excellent optical properties due to the synergistic effect of ceramic components and rough surface state.

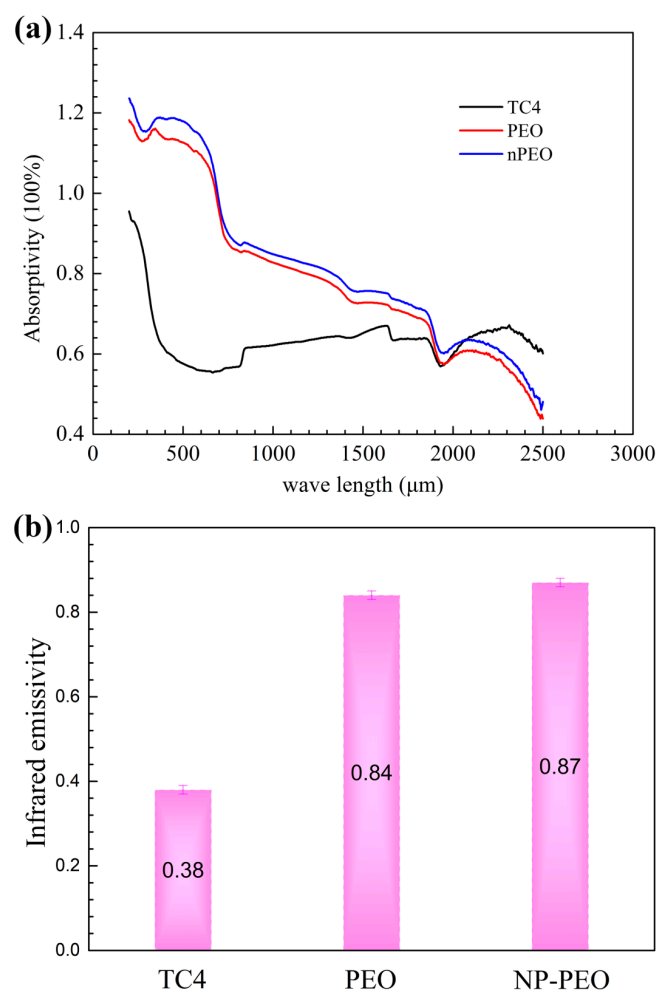


Figure 9. Optical properties of TC4 alloy and the PEO coatings. (a) Absorptivity and (b) emissivity.

4. Conclusions

Black PEO coating with MoSi₂ nanoparticles incorporation was fabricated on the surface of commercial TC4 alloy, with the aim of improving wear resistance and optical properties. The incorporated coating was characterized and the wear and optical properties of the coatings were investigated. The following conclusions can be drawn:

1. The incorporation of MoSi₂ particles increased the porosity of the PEO coating but decreased the average pore size (3.6 μm). The incorporation content increased with the prolongation of the deposition time.
2. Adhesion of particles impeded intensive discharge and thus presented lower surface roughness values (R_a 6.944 μm). The produced micro pores with smaller dimensions increased the hardness value of the nPEO coating.
3. PEO coating possessed larger surface roughness (R_a 8.307 μm), and presented relatively poor wear resistance. The addition of MoSi₂ particles remarkably improved the wear property of the PEO layer.
4. PEO coating exhibited higher absorptivity at most of the wavelength range, and the infrared emissivity increased from 0.38 to 0.84. The optical property was further improved after the incorporation of MoSi₂ particles.

Author Contributions: Conceptualization, H.Z.; methodology, J.H.; software, J.H.; validation, S.S.; formal analysis, J.X.; investigation, J.Z.; resources, J.H.; data curation, J.H.; writing—original draft preparation, H.Z.; writing—review and editing, H.Z.; visualization, J.H.; supervision, J.H.; project

administration, H.Z.; funding acquisition, H.Z. All authors have read and agreed to the published version of the manuscript.

Funding: This research was funded by the National Natural Science Foundation of China (52101286), Natural Foundation of Science and Technology Department of Sichuan Province (2024NSFSC0949), Sichuan Science and Technology Program (2023ZYD0115), and National College Student Innovation and Entrepreneurship Training Program (2024cxcy044, S202311360042).

Institutional Review Board Statement: Not applicable.

Informed Consent Statement: Not applicable.

Data Availability Statement: The data would be provided when is required.

Conflicts of Interest: The authors declare no conflicts of interest.

References

1. Le, T.; Lee, Y.; Tran, D.T.; Choi, W.S.; Kang, W.N.; Yun, J.; Kim, J.; Song, J.; Han, Y.; Park, T.; et al. Effect of C additives with 0.5 % in weight on structural, optical and superconducting properties of Ta–Nb–Hf–Zr–Ti high entropy alloy films. *J. Alloys Compd.* **2024**, *1008*, 176863. [\[CrossRef\]](#)
2. Lin, H.; Zhang, G.; Chen, W.; Zheng, K.; Yin, F. Design of new β -type Ti alloys with outstanding corrosion and wear resistance for dental application. *Corros. Sci.* **2024**, *241*, 112520. [\[CrossRef\]](#)
3. Eroshenko, A.Y.; Legostaeva, E.V.; Uvarkin, P.V.; Tolmachev, A.I.; Khimich, M.A.; Kuznetsov, V.P.; Stepanov, S.I.; Vorontsov, I.A.; Mukanov, G.Z.; Sharkeev, Y.P. Evolution of microstructure and mechanical properties of Ti–Nb–Zr and Ti–Nb–Zr–Ta–Sn alloys in severe plastic deformation. *Mater. Lett.* **2025**, *382*, 137805. [\[CrossRef\]](#)
4. Li, Z.; Fan, L.; Ma, L.; Duan, T.; Zhang, H.; Jian, H.; Sun, M. Perspective review on factors that influence the stress corrosion of Ti alloys for deep-sea applications. *J. Mater. Sci. Technol.* **2024**. [\[CrossRef\]](#)
5. Yao, W.; Li, X.; Wei, Q.; Fu, M.; Wang, B.; Pan, S. Oxidation behavior of TA15 titanium alloy at high-temperature and the effect on infrared emissivity. *J. Alloys Compd.* **2024**, *983*, 173707. [\[CrossRef\]](#)
6. Bai, L.-j.; Gao, X.; Luo, Y.; Chen, G.; Wu, X.; Sun, X. In-situ preparation of (Ti,Al) codoped blue PEO ceramic coating on magnesium alloy and chromogenic mechanism. *Surf. Coat. Technol.* **2023**, *470*, 129829. [\[CrossRef\]](#)
7. Madhuri, D.; Ghosh, R.; Hasan, M.A.; Dey, A.; Pillai, A.M.; Angamuthu, M.; Anantharaju, K.S.; Rajendra, A. Flat Absorber Black PEO coatings on Ti6Al4V for spacecraft thermal control application. *Ceram. Int.* **2022**, *48*, 35906–35914. [\[CrossRef\]](#)
8. Li, X.; Gao, X.; Liu, J.; Dong, J.; Wang, Y.; Chen, J.; Zhan, C.; Yin, Y.; Nan, D. Bi-functional epoxy coating with long-term protection for Q235 steel prepared by incorporating melamine-grafted and carbon-black-modified graphene oxide. *Surf. Coat. Technol.* **2024**, *485*, 130883. [\[CrossRef\]](#)
9. Jiang, X.; Yang, Y.; Qin, Z.; Jin, T.; Zhu, B.; Ren, L.; Jiang, L.; Liu, M.; Deng, Z.; Wei, G.; et al. Characterization of high absorbance and high-emissivity black NiCe oxide composite coatings produced via photo-assisted electrodeposition. *Surf. Coat. Technol.* **2023**, *454*, 129173. [\[CrossRef\]](#)
10. Yao, R.; Li, Y.; Yao, Z.; Zhang, P.; Lu, S.; Wu, X. Black PEO coating with enhanced thermal stability on titanium alloy and its thermal control properties. *Surf. Coat. Technol.* **2022**, *429*, 127934. [\[CrossRef\]](#)
11. Lim, S.-G.; Choe, H.-C. Bioactive apatite formation on PEO-treated Ti-6Al-4V alloy after 3rd anodic titanium oxidation. *Appl. Surf. Sci.* **2019**, *484*, 365–373. [\[CrossRef\]](#)
12. Hwang, I.-J.; Choe, H.-C. Effects of Zn and Si ions on the corrosion behaviors of PEO-treated Ti-6Al-4V alloy. *Appl. Surf. Sci.* **2019**, *477*, 79–90. [\[CrossRef\]](#)
13. Nadimi, M.; Dehghanian, C. Incorporation of ZnO–ZrO₂ nanoparticles into TiO₂ coatings obtained by PEO on Ti-6Al-4V substrate and evaluation of its corrosion behavior, microstructural and antibacterial effects exposed to SBF solution. *Ceram. Int.* **2021**, *47*, 33413–33425. [\[CrossRef\]](#)
14. Nisar, S.S.; Choe, H.-C. TiO₂ coatings doped with MoS₂ nanoparticles using plasma electrolytic oxidation on Ti-6Al-4V alloy: Application for enhanced and functional bio-implant surface. *J. Mater. Res. Technol.* **2024**, *33*, 2035–2056. [\[CrossRef\]](#)
15. Mashtalyar, D.V.; Imshinetskiy, I.M.; Kashepa, V.V.; Nadaraia, K.V.; Piatkova, M.A.; Pleshkova, A.I.; Fomenko, K.A.; Ustinov, A.Y.; Sinebryukhov, S.L.; Gnedenkov, S.V. Effect of Ta₂O₅ nanoparticles on bioactivity, composition, structure, in vitro and in vivo behavior of PEO coatings on Mg-alloy. *J. Magnes. Alloys* **2024**, *12*, 2360–2379. [\[CrossRef\]](#)
16. Nisar, S.S.; Choe, H.-C. Mechanical hydroxyapatite coatings on PEO-treated Ti-6Al-4V alloy for enhancing implant's surface bioactivity. *Ceram. Int.* **2024**, *50*, 17703–17719. [\[CrossRef\]](#)
17. Adigamova, M.V.; Malyshev, I.V.; Lukiyanchuk, I.V.; Tkachenko, I.A.; Saiankina, K.A. Effect of lanthanum manganite particles on the structure and magnetic behavior of PEO coatings on titanium. *Mater. Chem. Phys.* **2024**, *320*, 129479. [\[CrossRef\]](#)

18. Molaei, M.; Fattah-alhosseini, A.; Nouri, M.; Mahmoodi, P.; Nourian, A. Incorporating TiO₂ nanoparticles to enhance corrosion resistance, cytocompatibility, and antibacterial properties of PEO ceramic coatings on titanium. *Ceram. Int.* **2022**, *48*, 21005–21024. [[CrossRef](#)]
19. Fu, T.; Zhang, Y.; Chen, L.; Shen, F.; Zhu, J. Micromorphology evolution, growth mechanism, and oxidation behaviour of the silicon-rich MoSi₂ coating at 1200 °C in air. *J. Mater. Res. Technol.* **2024**, *29*, 491–503. [[CrossRef](#)]
20. Fu, T.; Zhang, Y.; Shen, F.; Cui, K.; Chen, L. Microstructure and oxidation behavior of Si-MoSi₂ coating deposited on Mo substrate at 600 °C and 900 °C in static air. *Mater. Charact.* **2022**, *192*, 112192. [[CrossRef](#)]
21. Zhu, L.; Chen, P.; Cai, Z.-M.; Feng, P.-Z.; Kang, X.-Q.; Akhtar, F.; Wang, X.-H. Fabrication of MoSi₂ coatings on molybdenum and its high-temperature anti-oxidation properties. *Trans. Nonferrous Met. Soc. China* **2022**, *32*, 935–946. [[CrossRef](#)]
22. Wang, J.; Chen, C.; Zhou, Y.; Wu, Z.; Gao, X.; Zhao, B.; Zhang, L.; Wang, H. An in-situ high-throughput study of the Invar effect in the Fe–Ni–Co system. *J. Alloys Compd.* **2025**, *1010*, 177755. [[CrossRef](#)]
23. Han, J.; Blawert, C.; Tang, S.; Yang, J.; Hu, J.; Zheludkevich, M.L. Formation and corrosion behaviors of calcium phosphate coatings on plasma electrolytic oxidized Mg under changing chemical environment. *Surf. Coat. Technol.* **2021**, *412*, 127030. [[CrossRef](#)]
24. Adigamova, M.V.; Lukiyanchuk, I.V.; Tkachenko, I.A.; Morozova, V.P. Fe-, Ni-containing ceramic-like PEO coatings on titanium and aluminum: Comparative analysis of the formation features, composition and ferromagnetic properties. *Mater. Chem. Phys.* **2022**, *275*, 125231. [[CrossRef](#)]
25. Han, J.; Yu, Y.; Yang, J.; Xiaopeng, L.; Blawert, C.; Zheludkevich, M.L. Corrosion and wear performance of La₂O₃ doped plasma electrolytic oxidation coating on pure Mg. *Surf. Coat. Technol.* **2022**, *433*, 128112. [[CrossRef](#)]
26. De Zanet, A.; Casalegno, V.; Cempura, G.; Malinverni, C.; Spriano, S.; Ferraris, S. TEM and zeta potential titration as suitable techniques for investigating the joining of modified ceramic surfaces. *Ceram. Int.* **2024**, *50*, 11787–11794. [[CrossRef](#)]
27. Jaleh, B.; Nasri, A.; Chaharmahali, R.; Kaseem, M.; Fattah-alhosseini, A. Exploring wear, corrosion, and microstructure in PEO coatings via laser surface treatments on aluminum substrates. *Opt. Laser Technol.* **2025**, *181*, 111958. [[CrossRef](#)]
28. Zhu, F.L.; Feng, Q.Q. Pore feature size influence on optical-infrared properties of porous polyamide film. *Mater. Lett.* **2023**, *346*, 134525. [[CrossRef](#)]
29. Yu, H.; Liang, W.; Miao, Q.; Yin, M.; Xu, Y.; Gao, J.; Jin, H.; Sun, S. High-temperature oxidation resistance and wear properties of functionally graded CrHfNbTaTiN high-entropy nitride coating on Ti alloy. *Appl. Surf. Sci.* **2025**, *680*, 161474. [[CrossRef](#)]
30. Tiwari, A.; Mishra, A.K.; Kumar, A. Influence of scan strategies on wear and tribological performance of Ti-6Al-4V alloy processed by laser powder bed additive manufacturing process. *Wear* **2025**, *562–563*, 205654. [[CrossRef](#)]
31. Yu, L.; Wang, M.; Hou, H.; Zhang, X.; Lei, S.; Liu, J.; Liu, G.; Qiao, G. Enhanced optical properties and mechanisms of Ba-doped LaMnO₃ perovskite ceramic coating. *Ceram. Int.* **2023**, *49*, 11696–11704. [[CrossRef](#)]
32. Charpentier, L.; Kauffmann, A.; Bêche, E.; Escape, C.; Laube, S.; Schliephake, D.; Esvan, J.; Gorr, B.; Soum-Glaude, A.; Heilmaier, M. Influence of the oxidation on the optical properties of Mo-Si-Ti, Ta-Mo-Cr-Al and Ta-Mo-Cr-Ti-Al alloys. *Mater. Today Commun.* **2023**, *37*, 107056. [[CrossRef](#)]

Disclaimer/Publisher’s Note: The statements, opinions and data contained in all publications are solely those of the individual author(s) and contributor(s) and not of MDPI and/or the editor(s). MDPI and/or the editor(s) disclaim responsibility for any injury to people or property resulting from any ideas, methods, instructions or products referred to in the content.